Science in China Series B: Chemistry

www.scichina.com
chem.scichina.com
www.springerlink.com

Quartz crystal microbalance study of the kinetics of surface initiated polymerization

CHEN XinAn[1], ZHANG YaoZhong[1], HE JianAn[1], XIONG ChunYang[1], MENG YongHong[2], JIN Gang[2] & MA HongWei[3†]

[1] Department of Biomedical Engineering, College of Engineering, Peking University, Beijing 100871, China;
[2] National Microgravity Laboratory, Institute of Mechanics, Chinese Academy of Sciences, Beijing 100190, China;
[3] Suzhou Institute of Nano-Tech and Nano-Bionics, Chinese Academy of Sciences, Suzhou 215125, China

Surface initiated polymerization (SIP) is a valuable tool in synthesizing functional polymer brushes, yet the kinetic understanding of SIP lags behind the development of its application. We apply quartz crystal microbalance (QCM) to address two issues that are not fully addressed yet play a central role in the rational design of functional polymer brushes, namely quantitative determination of the kinetics and the initiator efficiency (IE) of SIP. SIP are monitored online using QCM. Two quantitative frequency-thickness (*f*-*T*) relations make the direct determination and comparison of the rate of polymerization possible even for different monomers. Based on the bi-termination model, the kinetics of SIP is simply described by two variables, which are related to two polymerization constants, namely $a = 1/(k_{p,s,app}[M][R\cdot]_0)$ and $b = k_{t,s,app}/(k_{p,s,app}[M])$. Factors that could alter the kinetics of SIP are studied, including (i) the molecular weight of monomers, (ii) the solvent used, (iii) the initial density of the initiator, (iv) the concentration of monomer, [M], and (v) the catalyst system (ratio among the ingredients, metal, ligands, and additives). The dynamic nature of IE is also described by these two variables, $IE = al/(a + bt)$. Instead of the molecular weight and the polydispersity, we suggest that film thickness, the two kinetic parameters (*a* and *b*), and the initial density of the initiator and IE be the parameters that characterize ultra-thin polymer brushes. Besides the kinetics study of SIP, the reported method has many other applications, for example, in the fast screening of catalyst system for SIP and other polymerization systems.

surface initiated polymerization, quartz crystal microbalance, kinetics, controlled living radical polymerization

1 Introduction

Surface initiated polymerization (SIP) has made the preparation of ultra-thin polymer brushes a routine task, which now plays important roles in many fields of science and technology[1−3]. For example, polymer brushes via SIP rendered stability to dispersed nano-particles and colloids[4−9], minimized nonspecific protein adsorption, improved biocompatibility[10−15], and acted as matrix for biosensors[16−18] and separation applications[19−22]. SIP also opened new ways for nano/micro-fabrication[23−28], altered fluid behavior in nano/micro-fluidic devices[29−31], and was found in other exotic applications[32−35]. While pioneering reports dated back to the early 1980s[36,37], the renaissance of SIP began in 1998[2,3,19,37−40]. With more than ten years development, the research focus of SIP has now switched from proof-of-concept type demonstration of applications to finely tuning the structure of resulting films. This is because the performance of surface tethered polymer films depends heavily on the

Received March 21, 2009; accepted April 28, 2009
doi: 10.1007/s11426-009-0225-6
†Corresponding author (email: hwma2008@sinano.ac.cn)
Supported by the Nationd Natural Science Foundation of China (Grant No. 20604402), Natural Science Foundation of Beijing (Grant No. 2072008) and National Basic Research Program of Chian (Grant No. 2009CB320300)

structure[1,3], which makes the characterization a key issue. Furthermore, to realize rational design of functional coatings, the understanding of the performance-structure relation is critical.

Common surface characterization methods, such as XPS and TOF-SIMS, are useful in revealing surface chemistry for films prepared with both the "grafting to" and "grafting from" methods. The contact angle and the AFM measurements give surface energy and surface morphology (and other surface properties), respectively. Film thickness is another important physical index that characterizes surface coatings, which can be obtained by a number of methods such as AFM[41] and ellipsometry[42,43]. In the "grafting to" method, the tethered polymer chains are approximately treated the same as those free polymers in the grafting solution, which are typically characterized by parameters such as molecular weight (M_n, the number averaged molecular weight and M_w, the weight averaged one), polydispersity, and the degree of polymerization. Thus, the thickness is directly correlated with M_n[44]. By contrast, the "grafting from" method produces polymer chains on site without any references. There is no established method that can directly measure the M_n of surface tethered polymer films. Therefore, no correlation between film thickness and M_n is established. Jordan et al. first measured the swell ratio of polystyrene (PS) brushes (r = thickness in toluene/thickness in collapsed state) and then applied the self-consistent mean field theory to calculate the polymerization degree[37]. However, a direct correlation (i.e., an experimental method) is not trivial, mainly due to technical difficulties. Two strategies are currently in use that can correlate the thickness with M_n, namely the cleavage method and the solution approximation method.

In the cleavage method, one first synthesizes a thick polymer film on a large substrate, cleaves off polymer film from the substrate (by either HF or I_2 treatments), and then collects them for M_n measurements by GPC or other traditional methods[38,45]. Kim et al. reported that a 33.1 nm thick poly(methyl methacrylate) (PMMA) film had a M_n of 33100 g·mol^{-1}[46]. However, Matyjaszewski et al. calculated that a 100 nm thick polymer brush on a 1 cm^2 silicon wafer can only produce 10 μg mass, which was barely enough for GPC[40].

In the solution approximation method, sacrificial initiator is added to the polymerization solution so that polymerization proceeds both in solution and from the surface. Ejaz et al. reported a linear relation between the thickness of brush and M_n of free polymer in solution: the slope was ~3.8×10^{-4} nm/(g·mol^{-1}) for a glycopolymer[47]. Matyjaszewski reported a slope of ~4×10^{-4} nm/(g·mol^{-1}) for polystyrene (PS)[40]. Shah reported a slope of ~10^{-3} nm/(g·mol^{-1}) for PMMA[23], which agreed with Kim's result from the cleavage method[46]. A number of other research groups also provided experimental evidence that such approximation was consistent with the cleavage method[3,9]. Nevertheless, the difference in polymerization kinetics between a free space and a confined surface cannot be neglected. Jordan et al. argued that a curved surface might have different kinetics from a flat surface[37]. Moreover, while ellipsometry can easily measure films with a thickness down to the 1 nm level, polymers cleaved from such a thin film would be difficult to measure by GPC, and the size of substrate will be enormous. Therefore, there is a need to develop a third, independent method for the measurement of the molecular weight.

We recently applied quartz crystal microbalance (QCM) to determine the area averaged mass and viscoelasticity of the surface tethered polymer films (dry)[48]. If the number of growing sites (i.e., the initiator efficiency, IE) is accurately determined, M_n is easily calculated, for the area averaged mass increases which is shown in QCM study. Unfortunately, the determination of IE is one of the challenges not fully addressed in the field of SIP even after 10 years of intense research. Most of the information about IE was estimated from the M_n measurement and initiator density of a self-assembled monolayer (SAM, ~5.6 chain·nm^{-2}). Jordan et al. calculated the IE of PS brushes to be ~6% (~0.3 chain·nm^{-2}). Both Kim[46] and Shah[23] estimated the IE to be less than 10%, in agreement with the result by simulation that a high-density initiator layer does not ensure a dense polymer coating in the first place[40].

However, Huck and Baker found, under the same condition (i.e., from one batch), the thickness of PMMA brush increases as initiator density increases[49,50]. If the IE was less than 10%, the brush thickness on initial density of initiator would not have such dependence. Baker et al. attributed this to the island formation of the initiator/undecanthiol mixed SAMs[50]. This phenomenon was also monomer dependent because it was found that film thickness stopped increasing as the initiator density increased for the monomer oligo(ethylene glycol) methacrylate (OEGMA)[43]. Thus, the value of IE may be

determined by multiple factors and may vary throughout the course of polymerization. This dynamic nature would be revealed if one follows the SIP process in real time (i.e., to study the kinetics of SIP), which is another long-standing problem in the field of SIP.

Very few studies have tried to reveal the kinetics of SIP, mainly due to the lack of proper tools. This analytical challenge hinders further development of SIP[3]. NMR[9] and GPC[38,45] are two typical analytical tools for the kinetic studies of solution polymerization. Unfortunately, these methods are not applicable to SIP since all polymer chains are fixed on the surface in SIP. An alternative is to follow the kinetics of SIP offline, either by ellipsometry[50] or XPS[51]. Baker et al. determined the rate of polymerization (R_p) to be 1—10 nm·h^{-1} from ellipsometry data[50]. Several groups applied QCM[41,52−54] and cantilever[55] to online monitor SIP. We proposed in a previous report[54] that the linear frequency-thickness (*f*-*T*) relation could be applied to convert frequency decrease to thickness increase. Furthermore, the rate of polymerization was obtained in terms of thickness increase: $R_p = -dT/dt$, where T is the thickness of dry film and t is the time of polymerization. However, R_p, in terms of dT/dt, was not comparable among different monomers because the conversion factors (k_1, slope for the *f*-*T* relation) were monomer dependent. We reported herein a simple method for the direct determination of R_p in terms of the increase of area averaged monomer in number (10^{-12} mol·s^{-1}·mm^{-2}) for different monomers by QCM. We further developed a number of equations that enabled us to analyze other important factors that alter the kinetics of SIP such as the rate constants of polymerization and termination, as well as the initiator efficiency, which is the key to correlate M_n with film thickness.

2 Experimental

The initiator thiol (ω-mercaptoundecyl bromoisobutyrate) and QCM chips were received from HRBio (Beijing, China). Oligo(ethylene glycol) methacrylate (M_n = 526, 475 and 300, i.e., OEGMA526, OEGMA475 and OEGMA300) were purchased from Aldrich and used as received.

2.1 SIP in QCM

For OEGMA526, the process was as follows: the QCM chip modified with initiator thiol was placed in a Q-Sense E4 sensor (Q-Sense, Gothenburg, Sweden); then the activator generated by electron transfer (AGET)[56] in SIP was applied to grow polymer brushes. Incomplete reaction mixture (IRM) was the mixture of deoxygenated MilliQ-water and methanol. Complete reaction mixture (CRM) was composed of OEGMA526 (2 mL 4.2 mmol), $CuCl_2$ (0.7 mL 0.028 mmol), bipyridine (Bipy) (25 mg, 0.16 mmol), and ascorbic acid (AscA) (5 mg 0.028 mmol), with a mole ratio of monomer/$CuCl_2$/Bipy/AscA at 105/0.7/4/0.7 and a feed [$CuCl_2$] of 1.93 mM, unless otherwise indicated. The IRM and the composition of the CRM for other systems were shown in Table 1.

In a typical run of *in situ* SIP, the QCM was first primed with IRM till a stable baseline was established. Polymerization was initiated by pumping the CRM mixture to the sensor cell at a speed of 70 mL·h^{-1} for about 1 min, and then the speed was reduced to ~3 mL·h^{-1} after the exchange of IRM with CRM was completed (indicated by color change, from colorless to red in the lumen of the fluid tube). SIP was continued for a specified time (less than 200 min) at ~25℃ and monitored by QCM in real time. The polymerization was terminated by replacement of CRM with IRM, and rinsed with IRM till a stable baseline was reached. Samples were finally taken out of the sensor cell and rinsed with ethanol, MilliQ-water, and dried with flowing nitrogen before ellipsometry measurement.

After the 1st SIP, the polymer brushes of poly(OEGMA526) were functionalized with bromoisobutyryl bromide as the initiation moiety. Chips were immersed in CH_2Cl_2 (70 mL) at 0℃, and Et_3N (1.16 mL, 7 mmol) was added dropwise. After the mixture was stirred for about 10 min, we then added $BrCOC(CH_3)_2Br$ (0.88 mL, 7 mmol) dropwise into the mixture and stirred for another 30 min. The chips were then thoroughly rinsed with ethanol and MilliQ-water and dried with flowing nitrogen, followed by the 2nd SIP of OEGMA526 and ellipsometry measurement. For the 2nd SIP, the process was the same as the 1st SIP.

Experimental details for OEGMA300 and 475 could be found in early publications[48,54]. Briefly, AGET-SIP was applied to grow poly(OEGMA) brushes. IRM was deoxygenated and turned to MilliQ-water or the mixture of MilliQ-water and methanol. CRM was prepared by mixing well of two parts. Part 1 was prepared by adding a specified amount of $CuCl_2$/Bipy and a fixed amount of

Table 1 List of the experimental conditions for the three tested monomers

No.	Monomer [a]	Solvent (H_2O:MeOH) [b]	χ_I^{Sur} [c]	M/Cu^{II}/Asca/Bipy [d]	[M] ($mol \cdot L^{-1}$) [e]
1	300	1:0	1.00	175/1/0.7/4	0.54
2	475	1:0	1.00	114/1/0.7/4	0.35
3	475	1:0	0.42	114/1/0.7/4	0.35
4	475	1:0	0.15	114/1/0.7/4	0.35
5	526	1:1	1.00	105/0.7/0.7/4	0.33
6	526	1:4	1.00	95/0.7/0.7/4	0.30

a) OEGMA family, 300 stands for OEGMA300. b) The reaction mixture is a mixture of water and methanol in the volume ratio. c) The surface density of the initiator, determined by XPS measurement, see ref.[54] for details. d) M, Monomer, AscA, ascorbic acid, Bipy, bipyridine. e) The final concentration of monomer in the complete reaction mixture (CRM).

monomer to 5 mL IRM. Part 2 was prepared by adding a specified amount of AscA to 5 mL IRM. The two parts were mixed together in a glove box resulting in CRM, and we varied the ratio of monomer/$CuCl_2$/Bipy/AscA to investigate the influence of these factors on the polymerization process.

2.2 Ellipsometry

Film thickness was measured on an M-2000V spectroscopic ellipsometer (J. A. Woollam Co., Inc.) at angles of 65, 70 and 75° and wavelengths from 500 to 800 nm. Ellipsometric data were fitted for the thickness with material specific models in a vendor-supplied software, i.e., SAMs and poly(OEGMA) films with fixed (An, Bn) values of (1.45, 0.01) and (1.46, 0.01), respectively using a Cauchy layer model. The ellipsometric thickness for each sample was independently measured at six different locations and was reported as the average ± standard error.

2.3 Mathematical analysis

The moving window average method[51] is used to smooth the QCM curves, and then the curve of polymerization rate is obtained by applying a numerical differential[57] to each smoothed curve.

Statistical analyses were performed using a one-way analysis of variance (ANOVA) with Fisher's least significant difference PLSD post hoc test for multiple comparisons. *P*-values less than 0.05 were considered statistically significant. All calculations were performed using SPSS Software (Version 15.0; Chicago, IL).

3 Results and discussion

3.1 Experimental design

The experimental design was evolved from previous reports[48,54]. Briefly, an initiator functionalized QCM chip was first measured for its absolute resonating frequency in air (Scheme 1), which was automatically set to be the (0, 0) point. Second, IRM (incomplete reaction mixture) was introduced to the sensor chamber and the difference in frequency was read directly from the QCM curve. Third, the polymer brush was deposited via SIP in the QCM (i.e., online monitoring), resulting in Δf^{vi}. The resulting film was then measured for its dry thickness ($t_{f,dry}$) by ellipsometry. Finally, the now polymer coated QCM chip was measured for its absolute frequency, resulting in Δf^{iii}. Note that the frequency change (Δf) was named to be consistent with previous reports[48,54]. In this report, however, only the Δf^{iii} and Δf^{vi} were applied to study the kinetics of SIP.

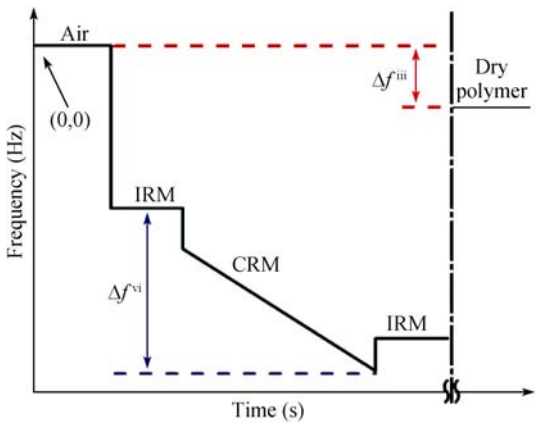

Scheme 1 Experimental design: SIP of OEGMA was conducted *in situ* in QCM and two frequency changes, namely Δf^{iii} and Δf^{vi}, were the key to the kinetic analysis. IRM, Incomplete reaction mixture; CRM, complete reaction mixture. See experimental section for details.

3.2 Empirical equations

Three monomers of the OEGMA family, namely OEGMA300, 475 and 526 were tested. The binary mixed self-assembled monolayers[58] of initiator (I) and undecanethiol (UDT, a dilutent) on gold were applied to

tune the initial density of initiator. Three initial densities of initiator ($\chi_I^{Sur} = M_I/(M_I+M_U)$, M is the number of molecules) were tested, namely 1.00, 0.42, and 0.15, where the values of χ_I^{Sur} were determined by XPS[43,54,59]. The frequency decreases were plotted against dry film thickness ($t_{f,dry}$), see Figure 1 for a representative plot for OEGMA526 (the reaction condition was listed in Table 1, No. 5) and see supplymentary materials Figure S1, S2 and S3 for plots for OEGMA475 and OEGMA300. For films below the 40 nm dry thickness limit, the following empirical equations were identified:

$$-\frac{\Delta f_n^{iii}}{n} = k_2 T \quad (1)$$

$$-\frac{\Delta f_n^{vi}}{n} = k_4 T + \frac{\Delta f_{n,IRM\to CRM}}{n}, \quad (2)$$

where n is the overtone number ($n=3$, corresponding to a resonating frequency at 15 MHz); k_2 and k_4 were experimentally determined values, the unit for k is Hz·nm^{-1}.

The k values of these linear f-T relations were listed in Table 2. In this study, the frequency change was a negative value for all the cases. For convenience, we applied $-\Delta f$ for figures. The value of $-\Delta f_{IRM\to CRM}$ was the frequency change due to solution exchange (i.e., from IRM to CRM in Scheme 1). It was a constant, i.e., ~143 Hz, ~188 Hz, and ~237 Hz for OEGMA300 (see supplementary materials Figure S4), OEGMA475, and OEGMA526, respectively. For eq. (1), the fit was forced to pass the origin point (0, 0) because the frequency change was zero when there was no polymer deposition. For eq. (2), the fit generated an intersection, which was due to the solution exchange (i.e., $-\Delta f_{IRM\to CRM}$).

From a previous study[48], we had eq. (3):

$$k_2 = 5.6\times10^{-3}\rho \quad (3),$$

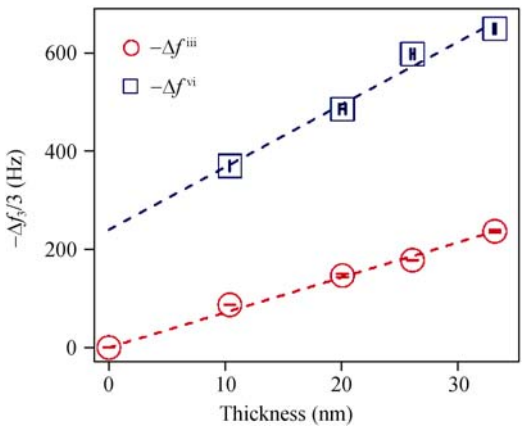

Figure 1 Linear relations between the frequency decreases and dry film thickness for poly(OEGMA526) under reaction condition No. 5 in Table 1. Representative f-t linear relations ($n=3$) with slopes of $k_2=7.12$ and $k_4=12.78$ for Δf^{iii} and Δf^{vi}, respectively (R^2 ~ 0.99). The intersection for the blue line is 237 Hz.

where ρ (kg m^{-3}) is the density of dry polymer deposited onto the QCM chip. We noticed that the values of k_2 were ~7 Hz·nm^{-1} for all three tested monomers, indicating that these polymers shared a similar density at their dried, collapsed states.

The values of k_4 were dependent on multiple factors: (i) k_4 was monomer dependent. Comparing OEGMA300 and 475, the higher M_w led to a higher k_4 value with all other conditions remaining the same (No.1 and No. 2 of Table 2); (ii) k_4 was initial initiator density dependent (Here we emphasize the term "initial" because the polymer chain density is determined not only by the initial initiator density but also by the initiator efficiency. We will come back to this point later). For OEGMA475, the lower the initial initiator density is, the higher k_4 value becomes; (iii) k_4 was solvent dependent (i.e., viscoelasticity dependent[48]). For OEGMA526, extra amount of methanol decreased the k_4 value. Furthermore, it was expected that OEGMA475 and 526 shared a similar k_4

Table 2 List of k values and other calculated constants for the three tested monomers

No.	Monomer [a]	Solvent (H_2O:MeOH) [b]	χ_I^{Sur} [c]	k_2 [d]	k_4 [e]	r [f]	r' [g]
1	300	1:0	1.00	6.96	11.57	0.60	0.36
2	475	1:0	1.00	7.19	14.68	0.49	0.18
3	475	1:0	0.42	6.65	16.88	0.39	0.15
4	475	1:0	0.15	7.15	18.75	0.38	0.14
5	526	1:1	1.00	7.12	12.78	0.56	0.19
6	526	1:4	1.00	7.27	11.57	0.63	0.21

a) OEGMA family, 300 stands for OEGMA300. b) The reaction mixture is a mixture of water and methanol in the volume ratio. c) The surface density of the initiator, determined by XPS measurement, see ref. [54] for details. d) Fitting results from eq. (1), in Hz nm^{-1}. e) Fitting results from eq. (2), in Hz nm^{-1}. f) $r=k_2/k_4$, see below for details of equation deduction. g) $r'=r/(5.6\times10^9 M_w)$, the unit is 10^{-12} mol·g^{-1}, see eq. (8) for details.

because these two monomers had similar M_w if the solvent was the same. However, the addition of methanol decreased the k_4 value significantly for OEGMA526 (Methanol was added because OEGMA526 did not dissolve well in water). These k_2 and k_4 values were applied to study the kinetics of SIP.

3.3 Equations for R_p analysis (differential analysis)

To compare R_p among different monomers, the following equations were deduced (see supplementary information for details for electronic version). The area averaged mass of dry polymer deposited onto the QCM chip can be calculated according to eq. (4):

$$\Delta\text{mass}_s = \rho T, \tag{4}$$

where the subscript s stands for surface confined, the unit for Δmass_s is kg·m^{-2}. Substituting eqs. (2) and (3) into (4), we had eq. (5):

$$\Delta\text{mass}_s = -\frac{r}{5.6\times10^{-3}}\left(\frac{\Delta f_n^{vi}}{n} - \frac{\Delta f_{n,\text{IRM}\to\text{CRM}}}{n}\right) \tag{5},$$

where $r = k_2/k_4$. Thus, we expressed the mass change in the term of Δf_n^{vi}, which could be applied for the kinetic study of SIP.

We further defined the rate of polymerization in terms of the increase of area averaged monomer in number as eq. (6). Substituting eq. (5) into (6), we had eq. (7):

$$R_{p,s} = \frac{d(\text{Mass}_s / M_w)}{dt} = \frac{1}{M_w}\frac{d\text{Mass}_s}{dt} \tag{6},$$

$$R_{p,s} = -r'\frac{d(\Delta f_n^{vi}/n)}{dt} \tag{7}$$

where Mass_s (g·mm^{-2}) was the area averaged mass, M_w (g·mol^{-1}) was the molecular weight of the tested monomer, t (s) was the polymerization time, $r' = r/(5.6\times10^9 M_w)$ was a molecular weight dependent constant, and $R_{p,s}$ (10^{-12} mol·s^{-1}·mm^{-2}) was an area averaged, monomer independent rate of polymerization.

Figure 2 presented a typical QCM curve and the corresponding $R_{p,s}$ curve according to eq. (7). Detailed reaction condition was listed as No. 5 in Table 1 and the resulting film thickness was 19.2 nm. The exchange of IRM with CRM led to dramatic frequency decrease (Figure 2(a)). We previously demonstrated that the addition of monomer to IRM would eliminate the large frequency decrease upon the exchange of IRM with CRM[56]. We did not add monomer to IRM because the fitting could remove the effect of solution exchange (see below).

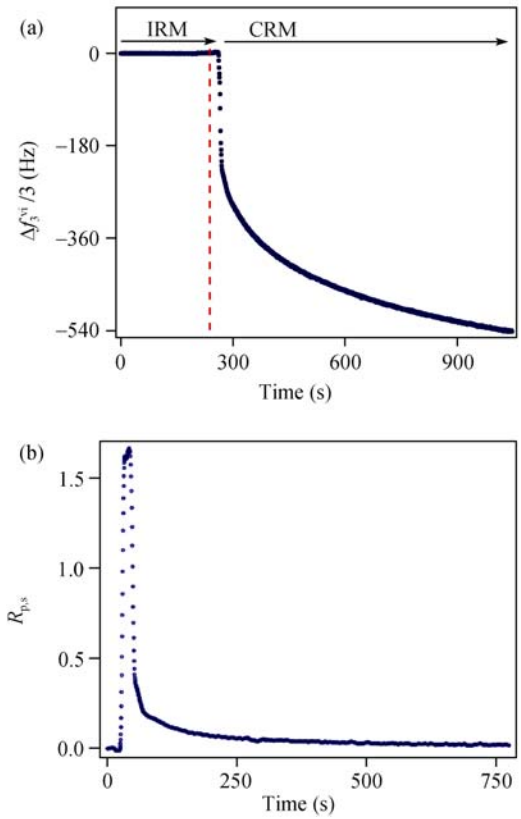

Figure 2 QCM enabled the determination of the polymerization rate ($R_{p,s}$). (a) SIP was monitored online by QCM: a representative QCM curve ($n = 3$) for monomer OEGMA475 under No. 5 reaction condition in Table 1. The final thickness was 19.2 nm. The red line indicated the time point, which was reset to zero for $R_{p,s}$ analysis. (b) Differentiation of the QCM curve (according to eq. (7)) gave the value of $R_{p,s}$ at each time point.

The red line in Figure 2(a) indicated where the time point was reset to zero for $R_{p,s}$ analysis. After differentiation according to eq. (7), the QCM curve was converted to a $R_{p,s}$ curve: the rate of polymerization was plotted against time (Figure 2(b)). The peak was due to the exchange of solution, which caused a ~200 Hz decrease within a few seconds, but the polymer deposition only led to a ~5 Hz decrease per second. Although the absolute value of $R_{p,s}$ was useful, this dynamic nature of $R_{p,s}$ values made the comparison among different runs of experiments difficult, which motivated us to further analyze this QCM curve based on the mechanism of free radical polymerization.

3.4 Data analysis based on the free radical polymerization mechanism (integral analysis)

Eq. (7) was deduced without the knowledge of the po-

lymerization mechanism. It provided us the $R_{p,s}$ value at each time point (Figure 2) but no insight information, for example, how the reaction condition (i.e., monomer, initiator density, solvent, and catalyst) affected the value of $R_{p,s}$. To obtain such information, the establishment of connection between eq. (7) and the polymerization mechanism would be first required.

For hundreds of runs of SIP, we observed no radical transfer in solution because no polymer was formed in solution. To simplify, we assumed that the surface confined polymerization was mechanistically the same as the solution polymerization was. Furthermore, we did not consider detailed mechanism of how the metal complex catalyzed this radical polymerization: whether it is ATRP mechanism[60] or SET mechanism[61]. And we only considered radical combination as the source of radical loss. Thus, we have eqs. (8) and (9):

$$R_{p,s} = k_{p,s,app}[M][R\cdot]; \tag{8}$$

$$\frac{d[R\cdot]}{dt} = -k_{t,s,app}[R\cdot]^2, \tag{9}$$

where $R_{p,s}$ (10^{-12} mol·s^{-1}·mm^{-2}) is the rate of polymerization; $k_{p,s,app}$ (mm^4·mol^{-1}·s^{-1}) and $k_{t,s,app}$ (M^{-1}·s^{-1}) are the apparent polymerization constant and termination constant, respectively; the subscript s represents surface confined, apprepresents apparent; [M] and [R·] are the concentration of monomer and radical, respectively. For the flow mode experiments and because of the extremely small amount of surface tethered initiators (6.5×10^{-10} mol for a QCM chip, see supplemental information for details for electronic version), one could take the following parameters as constants: [M] and the catalyst complex ([Cu^{II}] and [Cu^{I}] with ligands).

Note that the herein defined apparent polymerization constant $k_{p,s,app}$ (mm^4·mol^{-1}·s^{-1}) and termination constant $k_{t,s,app}$ (M^{-1}·s^{-1}) are different from those traditional ones, i.e., k_p (M^{-1}·s^{-1}) and k_t (M^{-1}·s^{-1}). The difference between $k_{p,s,app}$ and k_p is evident from their units: the difference is a thickness h (nm). For $k_{t,s,app}$ and k_t, the difference is due to the fact that [R·] for SIP was surface confined radicals. Furthermore, QCM detected the surface confined and area averaged mass change (2 dimensional, m^2), while the traditional methods detected the solution concentration change (3 dimensional volume, m^3), see supplemental information for details for electronic version.

From eq. (9), we have eq. (10):

$$[R\cdot] = \frac{[R\cdot]_0}{1 + k_{t,s,app}[R\cdot]_0 t}. \tag{10}$$

This is similar to the equation described by Patten et al.[62] and Xiao et al.[63] (developed from the solution phase polymerization) except the fact that the apparent termination constant ($k_{t,s,app}$) is for surface confined polymerization. Substituting (10) to (8), we have eqs. (11), (12) and (13) for $R_{p,s}$:

$$R_{p,s} = \frac{1}{a + bt}; \tag{11}$$

$$a = \frac{1}{k_{p,s,app}[M][R\cdot]_0}; \tag{12}$$

$$b = \frac{k_{t,s,app}}{k_{p,s,app}[M]} \tag{13}$$

where a and b have the units of 10^{12} mm^2·mol^{-1}·s and 10^{12} mm^2·mol^{-1}. Note that [M] is the monomer concentration and assumed to be homogenous (that is no near surface/interface effect); [R·] is the effective concentration of radical, which cannot be measured directly.

Integrating eq. (11), we have eq. (14)

$$\Delta\text{monomer}_s = \int_0^t R_{p,s}dt = \frac{1}{b}\ln(a + bt) + c \tag{14}$$

where Δmonomer$_s$ (10^{-12} mol·mm^{-2}) is the area averaged deposition, and c is the integral constant.

Eq. (14) was applied to fit the QCM curve. Figure 3 was a representative case for monomer OEGMA526, the detailed reaction condition was listed as No. 5 in Table 1. In Figure 3(a), the blue curve was the QCM curve. The red line indicated where the exchange of IRM with CRM was initiated, which was reset to be the (0,0) point for Figure 3(b). From eq. (5), we had eq. (15), which was monomer independent and applied to convert frequency changes to deposited monomer changes (in mole·mm^{-2}, the black curve in Figure 3(b)):

$$\Delta\text{monomer}_s = -r'\left(\frac{\Delta f_n^{vi}}{n} - \frac{\Delta f_{n,IRM\to CRM}}{n}\right) \tag{15}$$

Note that in Figure 3(b), we did not remove the frequency change due to solution exchange (i.e., $\Delta f_{IRM\to CRM}$), because it was included in the integral constant c in eq. (14) and could be removed subsequently. The red dots in Figure 3(b) were the fitted curve according to eq. (14). The fitted values of a, b, and c were listed as No. 3 in

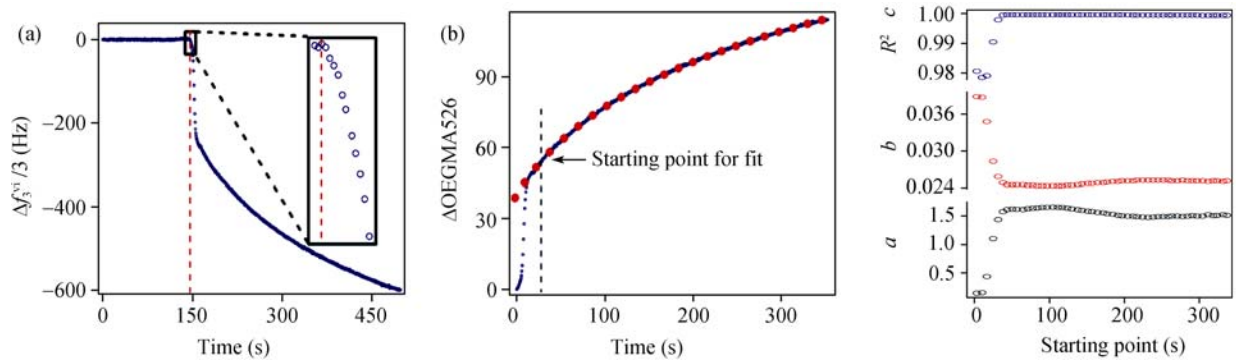

Figure 3 Kinetic analysis of SIP. (a) A representative *f*-*t* curve for OEGMA526, with an initial initiator density at 1.00 and a resulting dry film thickness at 26.1 nm (No. 5 in Table 1 and No. 3 in Table 3). Enlarged is the turning point that was set to be the (0,0) point for further analysis. (b) Fitting of a converted *f*-*t* curve according to eq. (14). (c) Error analysis indicated where to start fit and the point of diminishing of the interference due to the solution exchange ($\Delta f_{\mathrm{IRM}\to\mathrm{CRM}}$, see supplemental Figure S5 for electronic version for further discussion).

Table 3. It was practically difficult to completely separate the frequency decreases caused by solution exchange and polymerization. At the very beginning, frequency decrease due to solution exchange was dominant (~200 Hz decrease within a few seconds from solution exchange vs. ~5 Hz per second from polymerization). However, the duration of it was very short (see supplementary materials Figure S4 for electronic version), typically less than 30 s. The initiation of polymerization was instantaneous and the frequency decrease due to polymer deposition became dominant after ~30 s. This was also confirmed by the error analysis of the fitting (Figure 3(c)).

The fitted values of b were almost the same for all four samples, which was in agreement with eq. (13) in which b was determined by two constants ($k_{\mathrm{p,s,app}}$ and $k_{\mathrm{t,s,app}}$) and the monomer concentration, which was also constant throughout the course of polymerization. The values of a were found to vary substantially (up to 50%). From eq. (12), we proposed that this variation was due to the irreproducibility of the initiation step. Even though the initial concentration of initiator was the same for all four chips, the initial concentration of radical ($[R\cdot]_0$) could be very different due to unknown reasons. Previous results had also indicated that SIP could vary substantially[54] even under the same condition. We will discuss this further in the conclusion part.

The fitted values of c were not analyzed for three reasons: (i) we were unable to completely separate the frequency change due to solution exchange and polymer deposition, (ii) we were unable to precisely define the (0,0) point for the QCM curve (Figure 3(a)), which has significant impact on the c value fitting (but not much impact on the values of b), (iii) from eq. (14), at $t = 0$, there was no polymer deposition, and we had $\Delta\mathrm{monomer_s} = 0$. However, since we did not remove the $\Delta f_{\mathrm{IRM}\to\mathrm{CRM}}$ value from the QCM curve during the conversion (eq. (15), from Figure 3(a) to 3(b)), we expected to have $r'\Delta f_{\mathrm{IRM}\to\mathrm{CRM}} = c + \dfrac{\ln a}{b}$ as a constant, which was the case as listed in Table 3 (~35). Therefore, the fitted value c was a collection of many minor factors, such as the variation of $\Delta f_{\mathrm{IRM}\to\mathrm{CRM}}$ and operational variations (e.g., how the peristaltic pump was operated, see supplemental information for electronic version for details). From Table 3, the averaged value of $\Delta f_{\mathrm{IRM}\to\mathrm{CRM}}$ was ~183 Hz (convert factor was 0.19, from Table 2), which was close to ~230 Hz changed determined in control experiments (i.e., $\Delta f_{\mathrm{IRM}\to\mathrm{CRM}}$ measured from a bare QCM chip), indicating the analysis method was valid.

The fitted values of a and b for other monomers and polymerization conditions can be found in supplemental information (see supplementary materials Table S1—S5 for electronic version). The averaged values of a and b for each monomer were listed in Table 4. From eqs. (12) and (13), we had eqs. (16) and (17):

$$b[\mathrm{M}] = \frac{k_{\mathrm{t,s,app}}}{k_{\mathrm{p,s,app}}} \tag{16}$$

$$\frac{b}{a} = k_{\mathrm{t,s,app}}[\mathrm{R}\cdot]_0 \tag{17}$$

Eq. (16) gave the ratio between $k_{\mathrm{t,s,app}}$ and $k_{\mathrm{p,s,app}}$ and was independent of monomer concentration (useful for comparison between monomers).

Table 3 The fitted values of a and b according to eq. (14) for OEGMA526

No. [a]	Thickness (nm)	a	b	c	b[M] [b]	b/a [c]	$\frac{\ln a}{b}+c$ [d]
1	10.4	2.32	0.020	–9.54	0.0067	0.009	33.1
2	20.1	1.60	0.022	8.94	0.0073	0.014	30.3
3	26.1	1.66	0.024	19.22	0.0080	0.015	40.0
4	33.2	2.84	0.025	-6.72	0.0082	0.009	35.1

a) See No. 5 in Table 1 for details of the SIP condition. b) See eq. (16). c) See eq (17). d) The value of Δmonomer$_s$ at $t=0$, which is mainly due to $\Delta f_{IRM\rightarrow CRM}$.

Table 4 List of the average values of a and b for the three tested monomers

No.	Monomer	Solvent (H_2O∶MeOH)	χ_I^{Sur}	a_{ave} [a]	a_{SE} [b]	b_{ave} [c]	b_{ave}.[M] [d]
1	300	1∶0	1.00	1.42	0.79	0.017	0.0092
2	475	1∶0	1.00	0.98	0.22	0.064	0.022
3	475	1∶0	0.42	2.02	0.32	0.070	0.025
4	475	1∶0	0.15	3.04	0.76	0.073	0.025
5	526	1∶1	1.00	2.11	0.29	0.023	0.0075
6	526	1∶4	1.00	3.63	1.48	0.051	0.015

a) Averages of the fitted a according to eq. (14) for the tested monomers. b) The standard error of fitted a_{ave}. c) Averages of the fitted b, the SE for $b_{ave.}$ was very small, typically < 1%. d) Calculated according to eq. (16), b[M] = $k_{t,s,app}/k_{p,s,app}$.

3.5 Factors that alter the kinetics of SIP

From eqs. (12)—(14) and (16)—(17), we expected the following factors affect the kinetics of SIP, including (i) the molecular weight of monomers, (ii) the solvent used, (iii) the initial density of initiator, (iv) the concentration of monomer, [M], and (v) the catalyst system (ratio among the ingredients). These factors will be examined below so that the validation of these equations (i.e., the reported experimental and analytical methods) can be checked.

3.5.1 Impact of the molecular weight on the SIP kinetics. Monomer OEGMA300 and OEGMA475 are different only in their molecular weights (CH_2=C(CH_3)CO-(OCH_2CH_2)$_n$$OCH_3$), the former has n ~6 and the later has n ~9. Given all other reaction conditions the same (Table 1, No. 1 and No. 2), OEGMA475 has a value of $k_{t,s,app}/k_{p,s,app}$ that is 2.4-fold larger than that of OEGMA300 (Table 4, No. 1 vs. No. 2). One direct conclusion is that OEGMA300 polymerizes faster than OEGMA475 does, in other words, higher molecular weight reduces the rate of polymer growth. OEGMA526 has a molecular weight close to OEGMA475, however, the different SIP condition prevents the comparison between them (No. 2 and No. 5 in Table 1). With limited data here, we did not know if this was a consequence of the increased steric hindrance or was a consequence of the reduced reactivity of the vinyl group as the molecular weight increases. However, such a puzzle could be resolved using this reported method with a more detailed study.

3.5.2 Impact of solvent on the kinetics. Comparing the b[M] values of No. 5 and No. 6 in Table 4, we concluded that methanol could reduce the value of $k_{t,s,app}/k_{p,s,app}$. The SIP condition was listed as No. 5 and No. 6 in Table 1. Methanol was used to increase the solubility of monomer OEGMA526 (that is also the reason why there is no 1∶0 solvent condition for OEGMA526). The 1∶1 mixture of water and methanol set the b[M] value at 0.0075×10^9 m^{-1}, while the 1∶4 mixture set it at 0.015, which was a 2-fold increase. Water was known to accelerate the polymerization rate. For example, Baker et al. recently reported a ~300 nm film of OEGMA1100 using water as solvent[64]. From the limited data here, we knew that the composition of solvent could alter the value of $k_{t,s,app}/k_{p,s,app}$ but did not know if this was achieved via (i) increased reactivity of the vinyl group, (ii) altered catalytic performance of the catalyst, or (iii) a combination of these two mechanisms.

3.5.3 Impact of initial density of the initiator (radical concentration) on the kinetics. We first applied binary mixed SAM technique[58] to systematically vary the initial surface density of initiators: undecanethiol (U) was used as a dilutent to vary the initiator (I) density. In this study, three mixed SAMs with varied initiator density (χ_I^{Sur}) were subjected to SIP, namely, the 1.00, 0.42, and

0.15 density (No. 2−4 in Table 1). There was no significant difference of the b values among the 1.00, 0.42, and 0.15 initial density variation. This was expected because the initial density of initiator will not change the constants, $k_{t,s,app}$ and $k_{p,s,app}$. However, we found the values of a between 1.00 and 0.15 were statistically different (Figure 4). The a value of 0.15 density (3.04 ± 0.76) was statistically larger than that of 1.00 (0.98 ± 0.22), indicating the former had a smaller $[R\cdot]_0$ value. We noticed that the mixed SAM system had a limited capacity in tuning the initiator density: a 2-dimensional (2D) system with limited dynamic range (see supplemental information for electronic version for details). Thus, we applied the relayed SIP technique to enhance our ability of tuning the radical concentration[31].

In the relayed SIP design (Scheme 2), we conducted the 1st SIP from a 1.00 initiator SAM surface, with OEGMA526 as the monomer, (resulting OH group terminated polymer brushes). Next, the terminal OH groups were converted to initiation sites. Thus, one had a 3D presentation of initiators, which is of greater dynamic range. Finally, the 2nd SIP was conducted in QCM for kinetic analysis. Table 5 presented one example: the values of b[M] were again constant as expected. However, the a[M] values were significantly different: the increased number of initiators due to 3D presentation led to a 35-fold decrease of a[M] value. This decrease is greater than what the mixed SAM could achieve (a 3-fold decrease by increasing χ_I^{Sur} from 0.15 to 1.00). Note that in this relayed SIP format, we did not know the exact number of initiators for the 2nd SIP. This change of a[M] value may also partially due to the change of initiator presentation from 2D to 3D since it affects the accessibility of initiators/radicals to monomers partially due to the change of steric hindrance. From eq. (12), such impact is equivalent to a reduction in $[R\cdot]_0$, which leads to a larger a[M] value.

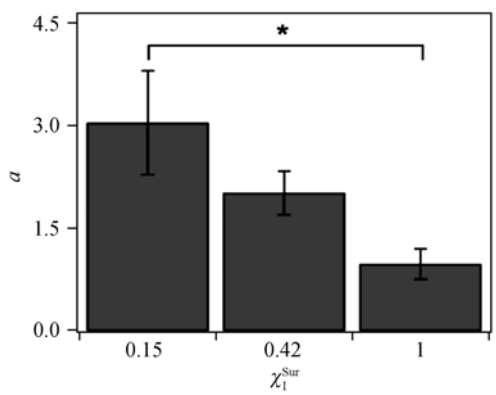

Figure 4 Statistical analyses were performed using a one-way analysis of variance (ANOVA) with Fisher's least significant difference PLSD post hoctest for multiple comparisons. For 1.00 and 0.42, $p = 0.115$; for 1.00 and 0.15, $p = 0.008$ (indicating significant difference); for 0.42 and 0.15, $p = 0.136$.

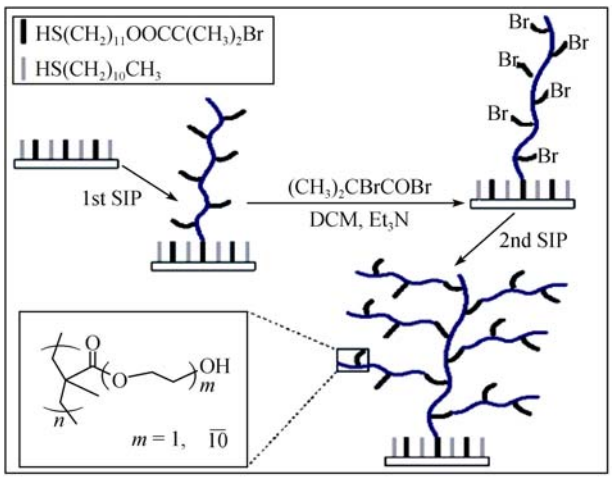

Scheme 2 Illustration of the relayed SIP process. The 1st SIP prepared a layer of poly(OEGMA526), which was used to anchor more initiation moieties. The 2nd SIP had a fast kinetics and resulted in polymeric trees.

3.5.4 Impact of the monomer concentration, [M]. Both eqs. (13) and (14) indicated the [M] could alter the value of a and b. We designed the following experiments to confirm this predication: all other experimental conditions were kept the same except the monomer concentration, [M], was varied as indicated in Table 6. Both a and b were decreased as [M] was increased. The values of b[M] were constant, agreed well with eq. (14). The values of a[M] were reasonably close given the large variation of a due to the irreproducibility of the initiation step. This partially proved the correctness of eqs. (13) and (14).

3.5.5 Impacts of the catalytic system. The catalytic system of the metal catalyzed living radical polymerization[59,65] is the key for the SIP. It typically consists of metal, ligand, and other additives. Optimization of its ingredient is of great importance to the development of this field and its industrial application[66]. We will demonstrate how this reported method (the QCM study of the kinetics of SIP) can be applied to optimize the catalytic system.

The CuBr/Bipy catalytic system led to a relatively slower polymer film growth and a smaller value of limit thickness when compared with the recently developed AGET SIP system (see supplemental information for

Table 5 The fitted values of *a* and *b* for the relayed SIP

SIP [a]	Thickness (nm) [b]	[M](mol·L^{-1}) [c]	*a*	*a*[M]	*b*	*b*[M]
1st	10.6	0.33	3.64	1.20	0.022	0.0072
2nd	51.9	0.18	0.20	0.035	0.041	0.0073

a) See No. 5 in Table 1 for the detailed SIP condition. b) For the 51.9 nm sample, we only fitted the first 40 nm range. c) The [M] was reduced to slow the polymerization rate.

Table 6 The monomer concentration alters the values of *a* and *b*

No.	[M] (mol·L^{-1}) [a]	*a*	*a*[M]	*b*	*b*[M]
1	0.18	8.9	1.58	0.125	0.022
2	0.35	1.1	0.39	0.067	0.024
3	0.57	1.2	0.66	0.038	0.022

a) See No. 2 in Table 1 for the detailed SIP condition except the monomer concentration was a variable.

electronic version)[67]. Matyjaszewski et al. further developed the so-called activator regenerated by electron transfer (ARGET) system, which differed from AGET only in the absolute amount of Cu^{II} used[66]. For the AGET and ARGET system, the catalyst consists of Cu^{II}, Bipy, and AscA. We will study these components individually.

First, we studied the impact of [Bipy]. It was clear from Table 7 that the increased [Bipy] led to smaller a values but constant *b* values. This indicated the fact that the increase of the polymerization rate was indeed due to the increased $[R\cdot]_0$ because [Bipy] did not affect the process of radical combination, i.e., $k_{t,s,app}$ did not change (eqs. (12) and (13)). To obtain the same information, traditional method required at least three runs of experiments to give a thickness-time plot.

Second, we studied the impact of the ratio of Cu(Ⅱ)/AscA. In Table 8, we kept the (initially added) amount of Cu^{II} constant and varied the amount of AscA.

Table 7 The bipyridine concentration alters the values of *a* and *b*

No.	[Bipy] [a]	*a*	*b*	*b*[M]
1	2	20.7	0.038	0.022
2	3	5.4	0.037	0.021
3	4	1.2	0.038	0.022
4	5	0.01	0.033	0.019

a) Monomer/Cu(Ⅱ)/AscA/Bipy = 200/1/0.7/Bipy (Bipy = 2, 3, 4, 5), [monomer] = 0.57 M.

Table 8 The ratio of Cu(Ⅱ)/AscA alters the values of *a* and *b*

No.	Cu(II)/AscA [a]	*a*	*b*	*b*[M]
1	1/0.3	97.4	0.035	0.020
2	1/0.5	27.9	0.032	0.018
3	1/0.7	20.7	0.038	0.022
4	1/0.9	16.2	0.034	0.019

a) monomer/Cu(Ⅱ)/AscA/Bipy = 200/1/AscA/2, [monomer] = 0.57 M.

As expected, the *b*[M] values were almost the same. The ratio of 1/0.3 was unique in that it gave a 5-fold higher value of *a* than the other three ratios were. Assuming the $k_{t,s,app}$ was kept constant (because the $k_{p,s,app}$ was the same), we concluded that $[R\cdot]_0$ was influenced by the ratio of Cu^{II}/AscA. Possible detailed mechanisms will not be discussed as it is beyond the scope of this paper.

The ratio of Cu^{II}/AscA listed in Table 8 was indeed for the AGET system. In Table 9, we found the difference between the ARGET and AGET systems. In ARGET system, the amount of AscA is more than that of Cu^{II} (No. 2 and No. 3 in Table 9). It was obvious that $k_{p,s,app}$ was not changed since *b*[M] was constant. The ratio of 0.2/0.7 set the fitted *a* value at 0.004, which was converted to a $[R\cdot]_0$ value that was impossible from an initiator SAM (The minimum value of *a* for an initiator SAM with 100% initiation rate was 1.9, see supplementaryl information for details). This is an indication that this reported method could be applied to explore the mechanism of metal catalyzed living radical polymerization.

Table 9 The ARGET vs. AGET

No.	Thickness (nm) [a]	Cu(Ⅱ)/AscA [b]	*a*	*b*[M]
1	23.2	1/0.7	20.7	0.022
2	45.4	0.5/0.7	6.5	0.023
3	122.8	0.2/0.7	0.004	0.019

a) Only the first 40 nm range was fitted. b) Monomer/Cu(Ⅱ)/AscA/Bipy = 200/Cu(Ⅱ)/0.7/2, [monomer] = 0.61 M.

To summarize, we demonstrated that the reported method (experimental design and data analysis) could predict how the following factors alter the kinetics of SIP, including (i) the molecular weight of monomers, (ii) the composition of solvent used, (iii) the initial density of initiator, (iv) the concentration of monomer, [M], and (v) the catalyst system (ratio among the ingredients). Such information will enhance our ability in rational design of functional surface coatings. Next, we will demonstrate how to use *a*, *b*, initiator efficiency (IE), and film thickness to characterize a surface tethered polymer film.

3.6 Initiator efficiency (IE)

One must be aware of the following facts: (i) not all initiators were activated and (ii) the number of growing sites was continuously declining, i.e., the initiator efficiency problem. Previous studies have also demonstrated that polymer density could be controlled by varying surface density of initiator in SIP, yet the final density of the film was difficult to determine[43,49,50].

From eq. (10), we have eq. (18):

$$\mathrm{IE}\% = \frac{[\mathrm{R}\cdot]}{[\mathrm{R}\cdot]_0} = \frac{a}{a+bt} = \frac{1}{1+\frac{b}{a}t} \tag{18}$$

In eq. (18), $[\mathrm{R}\cdot]$ is the live polymer chains and $[\mathrm{R}\cdot]_0$ is the total number of polymer chains. This IE is dynamic. The IE typically used in SIP research field as discussed in the introduction part is that: IE = polymer chains/total number of initiators, where the number of polymer chains was determined by GPC[23,40,46]. From this study, IE drops dramatically at the first 3 min, where polymer chains are still very short and not detectable by the GPC method. For the remaining period of SIP, the typical 10% IE value corresponds to long polymer chains and is detectable by GPC. Therefore, the physical meaning of IE defined by eq. (18) was the same with what is typically used.

From Table 3, $a \sim 2$ and $b \sim 0.02$, the value of IE% will reach 10% within 20 min (Figure 5(a)), which mathematically explained the reason why an IE% value of 5%—10% was typically identified[23,37,39]. Figure 5(a) also clearly demonstrated that the IE% were similar at the early and later stages for different runs but could be different in the middle of the SIP process, indicating a way of obtaining polymer brushes with subtle density difference.

Figure 5(b) was simulated to visualize how the variables a and b affect the SIP process. To obtain a dense polymer brush with limited density distribution at the Z-direction (perpendicular to the planar surface), one needs a relatively small b/a value, $\sim 10^{-7}$ (Figure 5(b)). From eqs. (12) and (13), $b/a = k_{\mathrm{t,s,app}}[\mathrm{R}\cdot]_0$, this indicated a small b/a value could be realized by using a catalytic system that gives a small $k_{\mathrm{t,s,app}}$ value or a small $[\mathrm{R}\cdot]_0$ value. The $[\mathrm{R}\cdot]_0$ value is determined by multiple factors, including (i) the initiator itself: benzyl alkyl halide is more reactive than tertiary butyl alkyl halide, while secondary alkyl halide is even less reactive than both the aforementioned[59], (ii) the catalytic system. For example, ARGET gave more $[\mathrm{R}\cdot]_0$ than AGET did as demonstrated above, (iii) the solvent used, and (iv) other minor factors such as oxygen level (due to leaking or incomplete purging at the very beginning) and temperature. It must be stated that a small $[\mathrm{R}\cdot]_0$ led to a slow R_{p}.

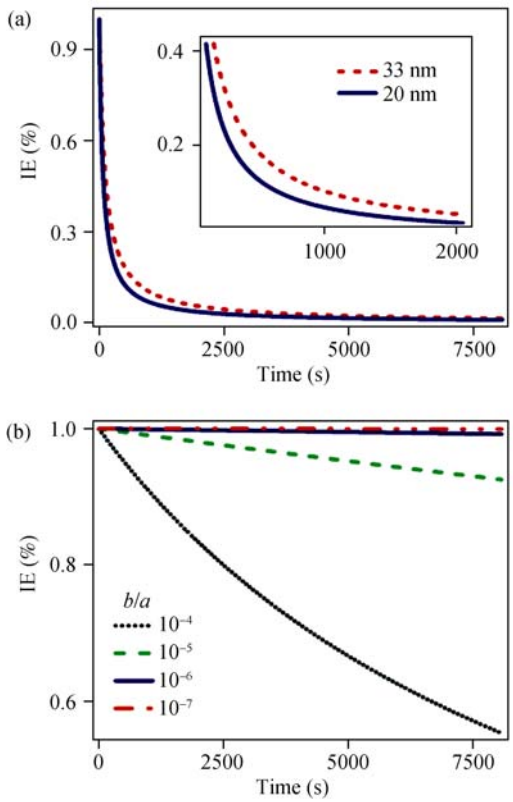

Figure 5 The dynamic nature of IE(%). (a) Representative plots of IE (%) against time according to eq. (18) for poly(OEGMA526). See text and Table 3 for details. (b) Simulation of the impact of the ratio of b/a on the IE according to eq. (18).

In Figure 6(a), we fixed b at 0.02 and varied a from 1 to 4. The rate of mass increase became similar for all four curves when t was larger than 400 s. And the difference in mass deposition was determined by the early period of polymerization ($t < 400$ s). A smaller a value could be realized through (we assumed [M] was kept constant): (i) increased $k_{\mathrm{p,s,app}}$ value but the ratio of $k_{\mathrm{t,s,app}}/k_{\mathrm{p,s,app}}$ was kept the same since b was kept constant, (ii) increased $k_{\mathrm{p,s,app}}[\mathrm{R}\cdot]_0$ value but the ratio of $k_{\mathrm{t,s,app}}/k_{\mathrm{p,s,app}}$ was kept the same since b was kept constant, (iii) increased $[\mathrm{R}\cdot]_0$ only. All three situations led to a faster polymerization rate and more mass deposition. Thus, the parameters a and b were instructive in designing SIP process.

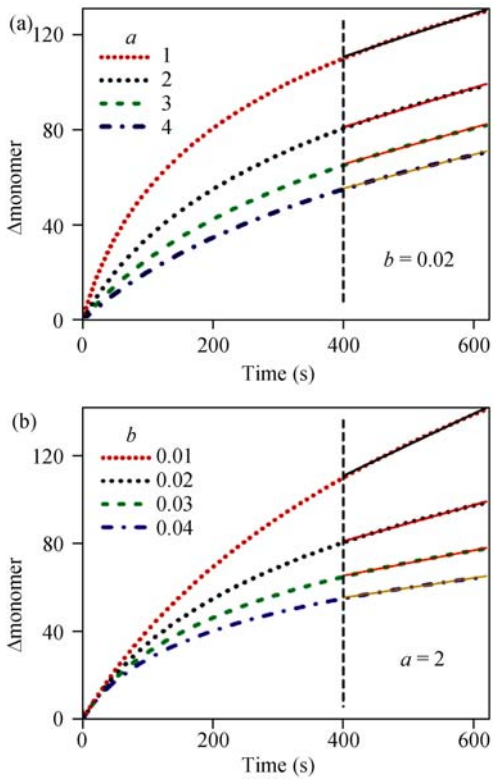

Figure 6 Simulations that show how the values of a and b affect the mass deposition. (a) Fixed a with varied b. (b) Fixed b with varied a, see text for details. The solid line after $t = 400$ s is only for the guide of eye for the comparison of slopes, assuming the curves became straight lines.

In Figure 6(b), we fixed the value of a at 2 and varied b from 0.01 to 0.04. It was clearly shown that b was the determining factor (for $t > 400$ s) for the deposition mass. A smaller b value (i.e., $k_{p,s,app} >> k_{t,s,app}$, we assumed [M] was kept constant) led to faster polymer deposition and the mass difference became larger as the polymerization time became longer. To summarize, IE not only depended on multiple factors but was also dynamic in nature, which made the determination of IE difficult and less meaningful. The dynamic nature of IE required the use of a tool that could follow the SIP in real time and QCM was proved to be one of the choices.

We have noticed subtle structural differences of polymer brushes from surfaces of close initial initiator density (only by QCM but not other methods, including AFM, XPS, and SEM, data now shown). Given our limited ability in characterizing polymer brushes with subtle difference, the variables a and b could present us a physical image of how the film was evolved. Thus, we propose that the film thickness and the two kinetic variables a and b could be used to characterize a polymer brush via SIP.

There are a few questions not addressed in this paper: (i) Persistent radical effect (PRE) is widely believed to play a central role in the metal catalyzed living radical polymerization system[68,69]. According to PRE, the concentration of radicals reaches its peak value after 10^{-2}—10^{-3} s of initiation, which is beyond the time resolution of QCM and our experimental design (the exchange of IRM with CRM takes ~ 30 s). The PRE also requires the accumulation of species that participate in the activation/deactivation balance. In our system, the flow mode does not meet this condition. Furthermore, the PRE states the resulted Cu^{II} is the main player. In our system, because of the extremely small amount of initiator immobilized on a QCM chip (1.3×10^{-7} mol of Cu^{II} from the SIP solution in the QCM chamber vs. 6.5×10^{-10} mol of Cu^{II} from the initiator if 100% conversion, see supplemental information for electronic version for details), the amount of the Cu^{II} produced by the PRE would not change the balance of activation/deactivation[63]. (ii) The individual determination of the values of $k_{t,s,app}$ and $k_{p,s,app}$ also requires further development of current protocol and even introduction of other techniques. These questions will be addressed in future publications.

4 Conclusions

We presented a QCM based method (experimental design and data analysis) to study the kinetics of SIP. Using QCM and ellipsometry, the kinetics of SIP could be described by two variables, namely $a = 1/(k_{p,s,app} \cdot [M][R\cdot]_0)$ and $b = k_{t,s,app}/(k_{p,s,app}[M])$. Fitting of the converted QCM curve according to eq. (14) gives reliable b value, and a smaller b value indicates faster SIP kinetics. The resulted a value shows variation, and it could only be used semi-quantitatively (supported by Figure 4). As pointed out previously, the irreproducibility of initiation step caused the variation of a. Such irreproducibility also existed in the batch mode because it is a problem of chemistry itself, not the experiment methods. We reasoned that batch mode did not reveal such irreproducibility because the very beginning period (less than a second as discussed above) could not be studied. In the batch mode, thickness was plotted against time, and the interval was typically 10 min or more. Although QCM was also unable to be used to directly study the events at the very first second, it was able to reveal the variation of $[R\cdot]_0$ by extrapolating to time zero (Figure 3(b)). Fur-

thermore, QCM results in late stages of SIP (after 10 min of initiation) agreed well with the batch mode. The establishment of such method makes it possible not only to optimize kinetics of SIP but also to study the mechanisms of SIP. This method has wide application potentials, including a fast screening of catalyst system[70] and studies of other interfacial phenomena that are associated with surface mass changes. Functional surface coatings via rational design aided by our reported method (optimized *a* and *b*) will be reported elsewhere.

We thank Mr. FU Long and Dou HaiQiang (Peking University) for conducting partial SIP experiment.

1 Jennings G K, Brantley E L. Physicochemical properties of surface-initiated polymer films in the modification and processing of materials. Adv Mater, 2004, 16(22): 1983－1994[DOI]

2 Edmondson S, Osborne V L, Huck W T S. Polymer brushes via surface-initiated polymerizations. Chem Soc Rev, 2004, 33(1), 14－22[DOI]

3 Tsujii Y O K, Yamamoto S, Goto A, Fukuda T. Adv Polym Sci, 2006, 197: 191－145

4 Pyun J, Matyjaszewski K. Synthesis of nanocomposite organic/inorganic hybrid materials using controlled/"living" radical polymerization. Chem Mater, 2001, 13(10): 3436－3448[DOI]

5 Vestal C R, Zhang Z J. Atom transfer radical polymerization synthesis and magnetic characterization of $MnFe_2O_4$/polystyrene core/shell nanoparticles. J Am Chem Soc, 2002, 124(48): 14312－14313[DOI]

6 Chen X Y, Armes S P, Greaves S J, Watts J F. Synthesis of hydrophilic polymer-grafted ultrafine inorganic oxide particles in protic media at ambient temperature via atom transfer radical polymerization: use of an electrostatically adsorbed polyelectrolytic macroinitiator. Langmuir, 2004, 20(3): 587－595[DOI]

7 Qin S H, Oin D Q, Ford W T, Resasco D E, Herrera J E. Polymer brushes on single-walled carbon nanotubes by atom transfer radical polymerization of *n*-butyl methacrylate. J Am Chem Soc, 2004, 126(1): 170－176[DOI]

8 Duan H W, Kuang M, Wang D Y, Kurth D G, Mohwald H. Colloidally stable amphibious nanocrystals derived from poly{[2-(dimethylamino)ethyl] methaerylatel capping. Angew Chem Int Ed, 2005, 44(11): 1717－1720[DOI]

9 Li D J, Sheng X, Zhao B. Environmentally responsive "Hairy" nanoparticles: Mixed homopolymer brushes on silica nanoparticles synthesized by living radical polymerization techniques. J Am Chem Soc, 2005, 127(17): 6248－6256[DOI]

10 Ma H W, Hyun J H, Stiller P, Chilkoti A. "Non-fouling" oligo(ethylene glycol)-functionalized polymer brushes synthesized by surface-initiated atom transfer radical polymerization. Adv Mater, 2004, 16(4): 338–341[DOI]

11 Fan X W, Lin L J, Dalsin J L, Messersmith P B. Biomimetic anchor for surface-initiated polymerization from metal substrates. J Am Chem Soc, 2005, 127(45): 15843－15847[DOI]

12 Yu W H, Kang E T, Neoh K G. Controlled grafting of comb copolymer brushes on poly(tetrafluoroethylene) films by surface-initiated living radical polymerizations. Langmuir, 2005, 21(1): 450－456[DOI]

13 Couet J, Jeyaprakash J D, Samuel S, Kopyshev A, Santer S, Biesalski M. Peptide-polymer hybrid nanotubes. Angew Chem Int Ed, 2005, 44(21): 3297－3301[DOI]

14 Heredia K L, Bontempo D, Ly T, Byers J T, Halstenberg S, Maynard H D. *In situ* preparation of protein－"Smart" polymer conjugates with retention of bioactivity. J Am Chem Soc, 2005, 127(48): 16955－16960[DOI]

15 Raynor J E, Petrie T A, Garcia A J, Collard D M. Controlling cell adhesion to titanium: Functionalization of poly[oligo(ethylene glycol)methacrylate] brushes with cell-adhesive peptides. Adv Mater, 2007, 19(13): 1724－1728[DOI]

16 Tugulu S, Arnold A, Sielaff I, Johnsson K, Klok H A. Protein-functionalized polymer brushes. Biomacromolecules, 2005, 6(3): 1602－1607[DOI]

17 Dai J H, Bao Z Y, Sun L, Hong S U, Baker G L, Bruening M L. High-capacity binding of proteins by poly(acrylic acid) brushes and their derivatives. Langmuir, 2006, 22(9): 4274－4281[DOI]

18 Zhang Z, Chao T, Chen S F, Jiang S Y. Superlow fouling sulfobetaine and carboxybetaine polymers on glass slides. Langmuir, 2006, 22(24): 10072－10077[DOI]

19 Huang X Y, Doneski L J, Wirth M J. Surface-confined living radical polymerization for coatings in capillary electrophoresis. Anal Chem, 1998, 70(19): 4023－4029[DOI]

20 Fu Q, Rao G V R, Ista L K, Wu Y, Andrzejewski B P, Sklar L A, Ward T L, Lopez G P. Control of molecular transport through stimuli-responsive ordered mesoporous materials. Adv Mater, 2003, 15(15): 1262－1266[DOI]

21 Carlmark A, Malmstrom E. Atom transfer radical polymerization from cellulose fibers at ambient temperature. J Am Chem Soc, 2002, 124(6): 900－901[DOI]

22 Wang H J, Zhou W H, Yin X F, Zhuang Z X, Yang H H, Wang X R. Template synthesized molecularly imprinted polymer nanotube membranes for chemical separations. J Am Chem Soc, 2006, 128(50): 15954－15955[DOI]

23 Shah R R, Merreceyes D, Husemann M, Rees I, Abbott N L, Hawker C J, Hedrick J L. Using atom transfer radical polymerization to amplify monolayers of initiators patterned by microcontact printing into polymer brushes for pattern transfer. Macromolecules, 2000, 33(2): 597－605[DOI]

24 von Werne T A, Germack D S, Hagberg E C, Sheares V V, Hawker C J, Carter K R. A versatile method for tuning the chemistry and size of nanoscopic features by living free radical polymerization. J Am Chem Soc, 2003, 125(13): 3831－3838[DOI]
25 Rutenberg I M, Scherman O A, Grubbs R H, Jiang W R, Garfunkel E, Bao Z. Synthesis of polymer dielectric layers for organic thin film transistors via surface-initiated ring-opening metathesis polymerization. J Am Chem Soc, 2004, 126(13): 4062－4063[DOI]
26 Mulvihill M J, Rupert B L, He R R, Hochbaum A, Arnold J, Yang P D. Synthesis of bifunctional polymer nanotubes from silicon nanowire templates via atom transfer radical polymerization. J Am Chem Soc, 2005, 127(46): 16040－16041[DOI]
27 Zhou F, Zheng Z J, Yu B, Liu W M, Huck W T S. Multicomponent polymer brushes. J Am Chem Soc, 2006, 128(50): 16253－16258[DOI]
28 Tsai Y S, Wang W C. Polybenzyl methacrylate brush used in the top-down/bottom-up approach for nanopatterning technology. J Appl Polym Sci, 2006, 101(3): 1953－1957[DOI]
29 Atencia J, Beebe D J. Controlled microfluidic interfaces. Nature, 2005, 437(7059): 648－655[DOI]
30 Whitesides G M. The origins and the future of microfluidics. Nature, 2006, 442(7101): 368－373[DOI]
31 Qian T C, Li Y F, Wu Y Z, Zheng B, Ma H W. Superhydrophobic poly(dimethylsiloxane) via surface-initiated polymerization with ultralow initiator density. Macromolecules, 2008, 41(18): 6641－6645[DOI]
32 Peng B, Ruhe J, Johannsmann D. Homogeneously aligned liquid-crystal polymer brushes. Adv Mater, 2000, 12(11): 821－824[DOI]
33 Bombalski L, Dong H C, Listak J, Matyjaszewski K, Bockstaller M R. Null-scattering hybrid particles using controlled radical polymerization. Adv Mater, 2007, 19(24): 4486－4490[DOI]
34 Tugulu S, Harms M, Fricke M, Volkmer D, Klok H A. Polymer brushes as ionotropic matrices for the directed fabrication of microstructured calcite thin films. Angew Chem Int Ed, 2006, 45(44): 7458－7461[DOI]
35 Lou X H, He L. DNA-accelerated atom transfer radical polymerization on a gold surface. Langmuir, 2006, 22(6): 2640－2646[DOI]
36 Vidal A, Guyot A, Kennedy J P. Silica-grafted polyisobutylene and butyl rubber .1. Synthesis and characterization of silica-grafted polyisobutylene. Polym Bull, 1980, 2(5): 315－320[DOI]
37 Jordan R, Ulman A, Kang J F, Rafailovich M H, Sokolov J. Surface-initiated anionic polymerization of styrene by means of self- assembled monolayers. J Am Chem Soc, 1999, 121(5): 1016－1022[DOI]
38 Prucker O, Ruhe J. Mechanism of radical chain polymerizations initiated by azo compounds covalently bound to the surface of spherical particles. Macromolecules, 1998, 31(3): 602－613[DOI]
39 Ejaz M, Yamamoto S, Ohno K, Tsujii Y, Fukuda T. Controlled graft polymerization of methyl methacrylate on silicon substrate by the combined use of the Langmuir-Blodgett and atom transfer radical polymerization techniques. Macromolecules, 1998, 31(17): 5934－5936[DOI]
40 Matyjaszewski K, Miller P J, Shukla N, Immaraporn B, Gelman A, Luokala B B, Siclovan T M, Kickelbick G, Vallant T, Hoffmann H, Pakula T. Polymers at interfaces: Using atom transfer radical polymerization in the controlled growth of homopolymers and block copolymers from silicon surfaces in the absence of untethered sacrificial initiator. Macromolecules, 1999, 32(26): 8716－8724[DOI]
41 Cheng N, Azzaroni O, Moya S, Huck W T S. The effect of [Cu-I]/[Cu-II] ratio on the kinetics and conformation of polyelectrolyte brushes by atom transfer radical polymerization. Macromol Rapid Comm, 2006, 27(19): 1632－1636[DOI]
42 Ruhe J. Polymers grafted from solid surfaces. Macromol Symp, 1998, 126: 215－222
43 Ma H W, Wells M, Beebe T P, Chilkoti A. Surface-initiated atom transfer radical polymerization of oligo(ethylene glycol) methyl methacrylate from a mixed self-assembled monolayer on gold. Adv Funct Mater, 2006, 16(5): 640－648[DOI]
44 Sofia S J, Premnath V, Merrill E W. Poly(ethylene oxide) grafted to silicon surfaces: Grafting density and protein adsorption. Macromolecules, 1998, 31(15): 5059－5070[DOI]
45 Husseman M, Malmstrom E E, McNamara M, Mate M, Mecerreyes D, Benoit D G, Hedrick J L, Mansky P, Huang E, Russell T P, Hawker C J. Controlled synthesis of polymer brushes by "Living" free radical polymerization techniques. Macromolecules, 1999, 32(5): 1424－1431[DOI]
46 Kim J B, Bruening M L, Baker G L. Surface-initiated atom transfer radical polymerization on gold at ambient temperature. J Am Chem Soc, 2000, 122(31): 7616－7617[DOI]
47 Ejaz M, Ohno K, Tsujii Y, Fukuda T. Controlled grafting of a well-defined glycopolymer on a solid surface by surface-initiated atom transfer radical polymerization. Macromolecules, 2000, 33(8): 2870－2874[DOI]
48 Fu L, Chen X N, He J N, Xiong C Y, Ma H W. Study viscoelasticity of ultrathin poly(oligo(ethylene glycol) methacrylate) brushes by a quartz crystal microbalance with dissipation. Langmuir, 2008, 24(12): 6100－6106[DOI]
49 Jones D M, Brown A A, Huck W T S. Surface-initiated polymerizations in aqueous media: Effect of initiator density. Langmuir, 2002, 18(4): 1265－1269[DOI]
50 Bao Z Y, Bruening M L, Baker G L. Control of the density of polymer brushes prepared by surface-initiated atom transfer radical polymerization. Macromolecules, 2006, 39(16): 5251－5258[DOI]
51 Burden R L, Faires J D. Numerical Analysis, 6th Ed. Singapore: Brooks-Cole Publishing Co, 1997
52 Moya S E, Brown A A, Azzaroni O, Huck W T S. Following polymer brush growth using the quartz crystal microbalance technique. Macromol Rapid Comm, 2005, 26(14): 1117－1121[DOI]
53 Ma H, Textor M, Clark R L, Chilkoti A. Monitoring kinetics of surface initiated atom transfer radical polymerization by quartz crystal microbalance with dissipation. Biointerphases, 2006, 1(1): 35－39[DOI]
54 He J, Wu Y Z, Wu J, Mao X, Fu L, Qian T C, Fang J, Xiong C Y, Xie J L,

Ma H W. Study and application of a linear frequency-thickness relation for surface-initiated atom transfer radical polymerization in a quartz crystal microbalance. Macromolecules, 2007, 40(9): 3090－3096[DOI]
55 Bumbu G G, Kircher G, Wolkenhauer M, Berger R, Gutmann J S. Synthesis and characterization of polymer brushes on micromechanical cantilevers. Macromol Chem Phys, 2004, 205(13): 1713－1720[DOI]
56 Matyjaszewski K, Dong H C, Jakubowski W, Pietrasik J, Kusumo A. Grafting from surfaces for "Everyone": ARGET ATRP in the presence of air. Langmuir, 2007, 23(8): 4528－4531[DOI]
57 Jones D M, Huck W T S. Controlled surface-initiated polymerizations in aqueous media. Adv Mater, 2001, 13(16): 1256－1259[DOI]
58 Bain C D, Evall J, Whitesides G M. Formation of monolayers by the coadsorption of thiols on gold－Variation in the head group, tail group, and solvent. J Am Chem Soc, 1989, 111(18): 7155－7164[DOI]
59 Matyjaszewski K, Xia J H. Atom transfer radical polymerization. Chem Rev, 2001, 101(9): 2921－2990[DOI]
60 Matyjaszewski K, Tsarevsky N V, Braunecker W A, Dong H, Huang J, Jakubowski W, Kwak Y, Nicolay R, Tang W, Yoon J A. Role of Cu-0 in controlled/"living" radical polymerization. Macromolecules, 2007, 40(22): 7795－7806[DOI]
61 Percec V, Guliashvili T, Ladislaw J S, Wistrand A, Stjerndahl A, Sienkowska M J, Monteiro M J, Sahoo S. Ultrafast synthesis of ultrahigh molar mass polymers by metal-catalyzed living radical polymerization of acrylates, methacrylates, and vinyl chloride mediated by SET at 25 degrees C. J Am Chem Soc, 2006, 128(43): 14156－14165[DOI]
62 Patten T E, Matyjaszewski K. Atom transfer radical polymerization and the synthesis of polymeric materials. Adv Mater, 1998, 10(12): 901－915[DOI]
63 Xiao D Q, Wirth M J. Kinetics of surface-initiated atom transfer radical polymerization of acrylamide on silica. Macromolecules, 2002, 35(8): 2919－2925[DOI]
64 Zheng Y, Bruening M L, Baker G L. Crystallization of polymer brushes with poly(ethylene oxide) side chains. Macromolecules, 2007, 40(23): 8212－8219[DOI]
65 Kamigaito M, Ando T, Sawamoto M. Metal-catalyzed living radical polymerization. Chem Rev, 2001, 101(12): 3689－3745[DOI]
66 Pintauer T, Matyjaszewski K. Atom transfer radical addition and polymerization reactions catalyzed by ppm amounts of copper complexes. Chem Soc Rev, 2008, 37(6): 1087－1097[DOI]
67 Oh J K, Min K, Matyjaszewski K. Preparation of poly(oligo(ethylene glycol) monomethyl ether methacrylate) by homogeneous aqueous AGET ATRP. Macromolecules, 2006, 39(9): 3161－3167[DOI]
68 Fischer H. The persistent radical effect in "living" radical polymerization. Macromolecules, 1997, 30(19): 5666－5672[DOI]
69 Zhang H Q, Klumperman B, Ming W H, Fischer H, van der Linde R. Effect of Cu(Ⅱ) on the kinetics of the homogeneous atom transfer radical polymerization of methyl methacrylate. Macromolecules, 2001, 34(18): 6169－6173[DOI]
70 Tang W, Kwak Y, Braunecker W, Tsarevsky N V, Coote M L, Matyjaszewski K. Understanding atom transfer radical polymerization: Effect of ligand and initiator structures on the equilibrium constants. J Am Chem Soc, 2008, 130(32): 10702－10713[DOI]

Supplementary materials

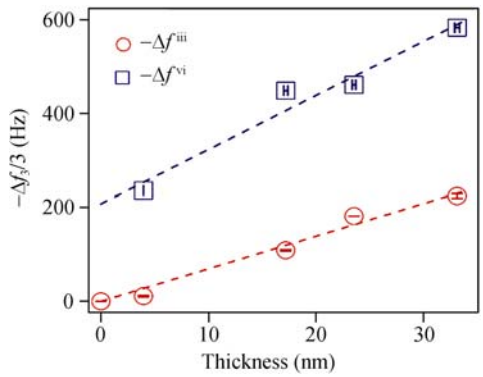

Figure S1 Linear relations between the frequency decreases and dry film thickness for poly(OEGMA300). Representative *f*-*T* linear relations ($n = 3$) with slopes of $k_2 = 6.96$ and $k_4 = 11.57$ for Δf^{iii} and Δf^{vi}, respectively ($R^2 \sim 0.99$).

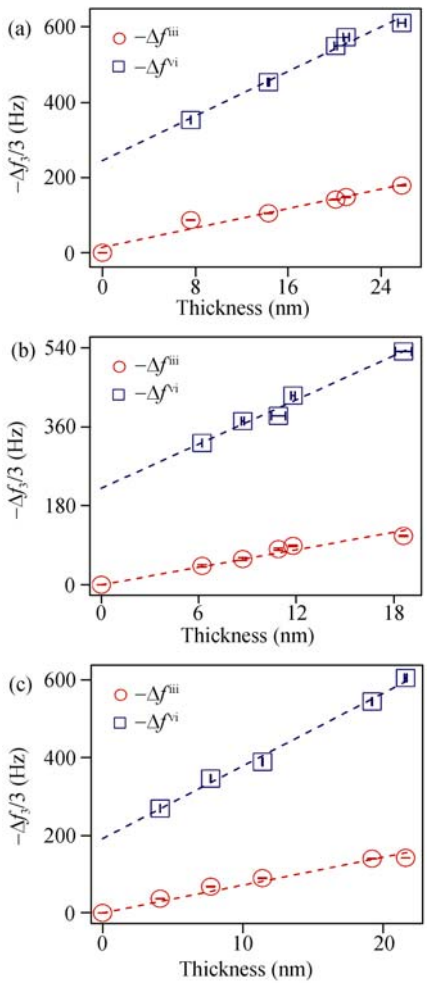

Figure S2 Linear relations between the frequency decreases and dry film thickness for poly(OEGMA475). See slopes of k_2 and k_4 for Δf^{iii} and Δf^{vi}, respectively, in Table 2. The initial initiator density was different: (a) 1.00, (b) 0.42, and (c) 0.15, $R^2 \sim 0.99$ for all six linear fittings.

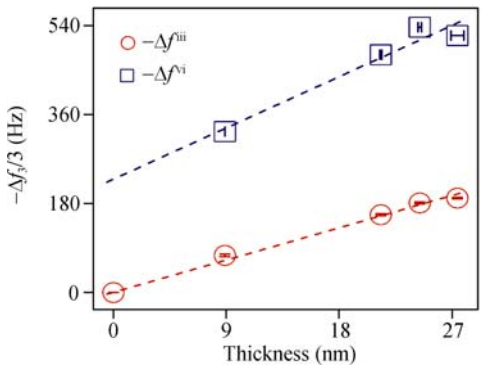

Figure S3 Linear relations between the frequency decreases and dry film thickness for poly(OEGMA526). Representative *f*-*T* linear relations ($n = 3$) with slopes of $k_2 = 7.37$ and $k_4 = 11.67$ for Δf^{iii} and Δf^{vi}, respectively ($R^2 \sim 0.99$, H_2O/MeOH = 1/4).

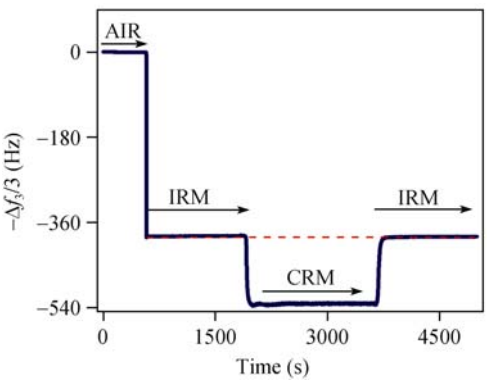

Figure S4 The frequency change due to exchange of IRM with CRM was a constant: ~143 Hz for OEGMA300 in water (see Table 1 in text for detailed conditions).

Detailed deduction of eq. (5)

From eq. (S1) and (S2):

$$k_2 = 5.6 \times 10^{-3} \rho \tag{S1}$$

Eq. (S1) corresponding to (3) in text.

$$\Delta\text{mass} = \rho T \tag{S2}$$

Eq. (S2) corresponding to (4) in text.

We can get eq. (S3):

$$\Delta\text{mass}_s = \frac{k_2}{5.6 \times 10^{-3}} T \tag{S3}$$

Substituting eq. (S3) into (S4), we had eq. (S5):

$$-\frac{\Delta f_n^{iii}}{n} = k_2 T \tag{S4}$$

Eq. (S4) corresponding to (1) in text.

$$\Delta\text{mass}_\text{s} = -\frac{\Delta f_\text{n}^{\text{iii}}/n}{5.6\times10^{-3}} \quad \text{(S5)}$$

From eq. (S4) and (S6), we have eq. (S7):

$$-\frac{\Delta f_\text{n}^{\text{vi}}}{n} = k_4 T + \frac{\Delta f_{\text{n,IRM}\to\text{CRM}}}{n} \quad \text{(S6)}$$

Eq. (S6) corresponding to (2) in text.

$$\frac{\Delta f_\text{n}^{\text{iii}}/\text{n}}{k_2} = \frac{\Delta f_\text{n}^{\text{vi}}/n + \Delta f_{\text{n,IRM}\to\text{CRM}}/n}{k_4} \quad \text{(S7)}$$

For further deduction, we have eq. (S8):

$$\Delta\text{mass}_\text{s} = -\frac{k_2/k_4}{5.6\times10^{-3}}\left(\frac{\Delta f_\text{n}^{\text{vi}}}{n} + \frac{\Delta f_{\text{n,IRM}\to\text{CRM}}}{n}\right) \quad \text{(S8)}$$

Let $r = \frac{k_2}{k_4}$. Then

$$\Delta\text{mass}_\text{s} = -\frac{r}{5.6\times10^{-3}}\left(\frac{\Delta f_\text{n}^{\text{vi}}}{n} + \frac{\Delta f_{\text{n,IRM}\to\text{CRM}}}{n}\right) \quad \text{(S9)}$$

Eq. (S9) corresponding to eq. (5) in text.

Compare the difference between the bulk phase and surface phase

Differential analysis: define the rate of polymerization ($R_{\text{p,s}}$) as the increase of monomers in unit time and unit surface area (surface phase).

$$R_{p,s} = \frac{\text{d}\left(\text{Mass}/M_w\right)}{\text{d}t} = \frac{\text{dMass}}{M_w \text{d}t}$$

Compare R_p from the bulk phase and the surface phase: bulk phase, R_p in mole·(dm^{-3})·s^{-1} ≡ 10^3 mole·m^{-3}·s^{-1}; surface phase, $R_{\text{p,s}}$ in mole·(mm^{-2})·s^{-1} ≡ 10^4 mole m^{-2}·s^{-1}. The difference of these two is the h (height):

$$R_\text{p} = \frac{R_{\text{p,s}}}{h} \quad (h \text{ in m})$$

Integral analysis: compare the Δmonomer from the bulk phase and the surface phase: bulk phase, Δmonomer in mole L^{-1} ≡ 10^3 mole·m^{-3}; surface phase, $\Delta\text{monomer}_\text{s}$ in mole mm^{-2} ≡ 10^4 mole·m^{-2}. The difference of these two is also the h (height):

$$\Delta\text{monomer} = \frac{\Delta\text{monomer}_\text{s}}{h}$$

One may suggest to define h as the convert factor from the bulk phase to the surface phase, and it contains several factors, such as $[\text{M}]\to[\text{M}]_\text{s}$, $[\text{R}\cdot]\to[\text{R}\cdot]_\text{s}$, $k_\text{p}\to k_{\text{p,s}}$ and $k_\text{t}\to k_{\text{t,s}}$.

Assuming the bi-termination mechanism of the (free) radicals, first consider the situation in the bulk phase:

$$R_\text{p} = k_\text{p}[\text{M}][\text{R}\cdot]$$

k_p in M^{-1}·s^{-1}, [M] and [R·] in M (mol·L^{-1}).

$$\Delta\text{monomer} = \frac{1}{b}\ln(a+bt) + c$$

Then, consider the fact that QCM detects surface confined, area averaged mass,

$$R_{\text{p,s}} = k_{\text{p,s,app}}[\text{M}]_\text{s}[\text{R}\cdot]_\text{s}$$

$$R_{\text{p,s}} = k_\text{p}[\text{M}][\text{R}\cdot]h$$

$$\frac{\text{d}[\text{R}\cdot]}{\text{d}t} = k_\text{t}[\text{R}\cdot]^2$$

$$[\text{R}\cdot] = \frac{[\text{R}\cdot]_0}{1+k_\text{t}[\text{R}\cdot]_0 t}$$

$$R_{\text{p,s}} = \frac{k_\text{p}[\text{M}][\text{R}\cdot]_0 h}{1+k_\text{t}[\text{R}\cdot]_0 t} = \frac{1}{a+bt}$$

$$a = \frac{1}{k_\text{p}[\text{M}][\text{R}\cdot]_0 h}, \quad b = \frac{k_\text{t}}{k_\text{p}[\text{M}]\cdot h}$$

$$\Delta\text{monomer}_\text{s} = \Delta\text{monomer}\cdot h = h\left[\frac{1}{b}\ln(a+bt)+c\right]$$

The difficulty is then how to define the value of h (this will be addressed at the end of this material).

How to choose the range for fitting: Further mathematical transformation led eq. (14) to have the following form:

$$\Delta\text{monomer}_\text{s} = \frac{1}{b}\ln\left(t+\frac{a}{b}\right) + \left(c+\frac{\ln b}{b}\right)$$

It was clear from the above equation that the variable b determined the shape of the curve (i.e., the converted QCM curve, $\Delta\text{monomer}_\text{s}$), the variable a/b determined the shift at the X-axis (i.e., time), and the variable $c+\frac{\ln b}{b}$ reflected the shift at the Y-axis (i.e., Δmonomers). The shape of the curve was relatively easy to define (a wide time window). The (0,0) point was also relatively easy to define as the enlarged area of Figure S5(a) usually shown a sharp turn. The shift at the Y-axis, however, was difficult to determine as it was affected by many

factors. This led to the variable c with no use. Fortunately, the variable c did not contain much information for the kinetics.

Figure S5 clearly demonstrated that the error analysis (Figure S5(c)) could help us chose the right time point to start fit. If one chose a start point that was within the mixed area (solution exchange mixed with polymer growth, < 30 s), the R^2 indicated a bad fitting. Similarly, if one chose a start point that was far away from the real starting point, the R^2 dropped again because the SIP might deviate from the bi-termination mechanism (other factors such as oxygen induced termination).

Now we discuss the criteria of defining the fitting range: (i) The starting point is determined based on two conditions, first is to pass the solution exchange period, i.e., > 30 s; second is a stable (~100 s) R^2 value > 0.98,

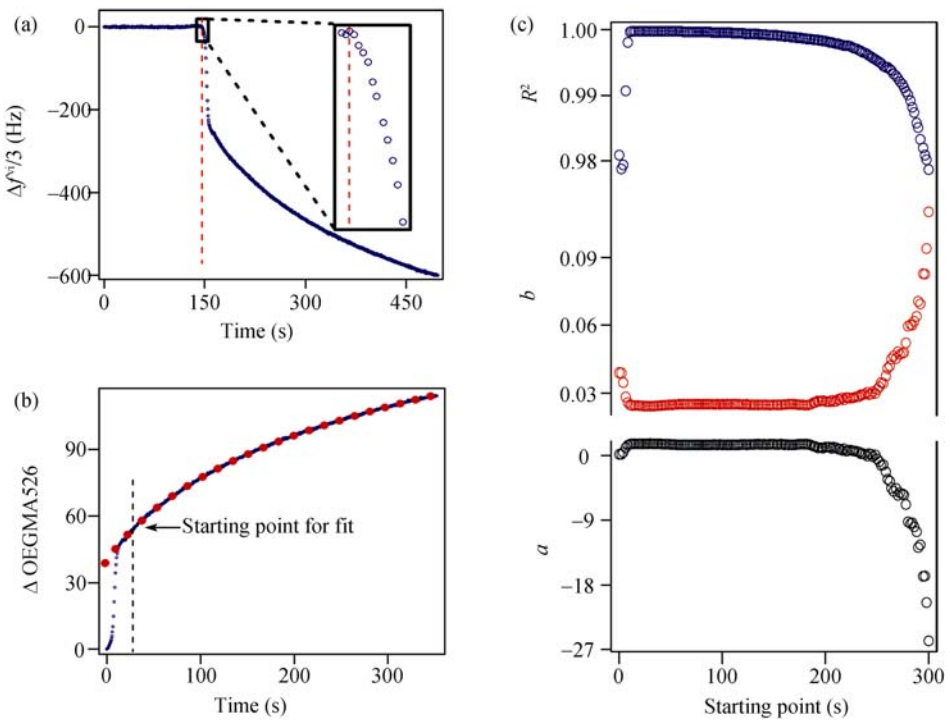

Figure S5 Kinetic analysis of SIP. (a) A representative *f*-*t* curve for OEGMA526, with an initial initiator density at 1.00 and a dry film thickness at 26.1 nm (No. 5 in Table 1 and No. 3 in Table 3), enlarged is the turning point that was set to be the (0,0) point for analysis. (b) Fitting of the converted *f*-*t* curve according to eq. (14). (c) Error analysis indicated where to start fit and the point of diminishing of the interference due to the solution exchange ($\Delta f_{IRM\rightarrow CRM}$).

List of the detailed fitted values.

Table S1 The fitted values of a and b according to eq. (14) for OEGMA526

No. [a]	Thickness (nm)	a	b	c	b[M] [b]	b/a [c]
1	8.9	1.28	0.051	35.3	0.015	0.040
2	21.3	5.40	0.054	23.0	0.016	0.010
3	24.4	1.10	0.054	38.5	0.015	0.049
4	27.4	7.40	0.053	7.0	0.015	0.007

a) See No. 6 of Table 1 for details of the reaction condition, b) See eq. (16). c) See eq. (17).

Table S2 The fitted values of a and b according to eq. (14) for OEGMA475 ($\chi_1^{Sur} = 1.00$)

No. [a]	Thickness (nm)	a	b	c	b[M] [b]	b/a [c]
1	7.6	1.57	0.065	24.9	0.023	0.041
2	14.3	1.26	0.065	23.5	0.023	0.051
3	20.1	0.56	0.061	47.4	0.021	0.110
4	21.0	0.40	0.063	36.8	0.022	0.157
5	25.8	1.13	0.067	21.1	0.024	0.060

a) Initial density of the initiator at 1.00. See No. 2 of Table 1 for details of the reaction condition. b) See eq. (16). c) See eq. (17).

Table S3 The fitted values of *a* and *b* according to eq. (14) for OEGMA475 ($\chi_1^{Sur} = 0.42$)

No. [a]	Thickness (nm)	*a*	*b*	*c*	*b*[M] [b]	*b*/*a* [c]
1	6.2	2.17	0.072	17.0	0.025	0.033
2	8.7	2.47	0.069	7.9	0.024	0.028
3	10.9	1.28	0.069	21.6	0.024	0.054
4	11.8	2.88	0.071	13.2	0.025	0.024
5	18.6	1.28	0.070	12.7	0.024	0.055

a) Initial density of the initiator at 0.42. See No. 3 of Table 1 for details of the reaction condition. b) See eq. (16), c) See eq. (17).

Table S4 The fitted values of *a* and *b* according to eq. (14) for OEGMA475 ($\chi_1^{Sur} = 0.15$)

No. [a]	Thickness (nm)	*a*	*b*	*c*	*b*[M] [b]	*b*/*a* [c]
1	7.7	4.60	0.073	7.27	0.025	0.016
2	11.4	1.44	0.073	18.84	0.026	0.051
3	19.2	2.08	0.071	19.07	0.025	0.034
4	21.6	4.06	0.074	10.36	0.026	0.018

a) Initial density of the initiator at 0.15. See No. 4 of Table 1 for details of the reaction condition. b) See eq. (16). c) See eq. (17).

Table S5 The fitted values of *a* and *b* according to eq. (14) for OEGMA300.

No. [a]	Thickness (nm)	*a*	*b*	*c*	*b*[M] [b]	*b*/*a* [c]
1	4.0	3.74	0.016	-33.95	0.008	0.004
2	17.2	0.27	0.018	84.03	0.010	0.066
3	23.5	0.64	0.017	70.62	0.009	0.027
4	33.1	1.02	0.017	48.24	0.009	0.017

a) See No. 1 of Table 1 for details of the reaction condition. b) See eq. (16), c) See eq (17).

(ii) The ending point is chosen so that the frequency change (i.e., the film thickness) is within the linear *f*-*t* relation range. There are SIP conditions that have fast kinetics and deposit more than 100 nm polymer film within a few minutes. For those experiments, the fitting range must be narrowed, (iii) One must also pay attention to the overall reaction time. The catalyst system applied is sensitive to oxygen and long reaction time (situations where we used a SIP condition of slow growth rate) will inevitably lead to oxygen leaking therefore deviate from the bi-termination model, (iv) Other factors such as the baseline shifting may play significant role for long polymerization period, especially the later stage that usually has very small frequency decrease rate.

The initiator on QCM chips:

The gold coated area of a QCM chip is a circle with a diameter of 10 mm.

The surface area occupied by an initiator molecule: S_0 ~20 Å^2[1]

The surface area of a QCM chip: $S_1 = \left(\frac{D}{2}\right)^2 \pi$

The amount of the initiator (*n*) on a QCM chip was calculated by $n = \frac{S_1}{S_0 N_A}$, where N_A is the Avogadro's constant.

$$n_{\text{initiator}} = \frac{(5\times10^{-3})^2 \times 3.14}{20\times10^{-20}\times 6.02\times10^{23}} = 6.5\times10^{-10}\,(\text{mol})$$

The concentration of Cu (refer to the element of Cu, for the added AscA will convert part of Cu^{II} to Cu^{I}) is 3.2×10^{-3} M, which gives 1.3×10^{-7} mol of Cu in the 40 μL QCM chamber. Comparing the absolute amount of initiator and Cu in the QCM chamber, we found n_{Cu} ~$500n_{initiator}$, so the initiator can hardly influence the balance of catalyst activation and deactivation ($Cu^{II} \leftrightarrow Cu^{I}$).

The estimation of *h*

One can estimate the value of *h* by evaluating the resulting constants of k_p or k_t. If the constants are physically reasonable, then the estimated value of *h* is also reasonable. Wet first assume that k_p is the same with the solution phase, that is 3.6×10^3 $M^{-1}\cdot s^{-1}$[2,3]. From equa-

tions (12) and (13), we can calculate the value of k_t and $[R\cdot]_0$. The result is listed in Table S6.

Table S6 The calculation of $[R\cdot]_0$ and k_t for OEGMA475 ($\chi_1^{Sur} = 1.00$).

No.	Thickness (nm)	$h = 20$ nm		$h = 2$ nm	
		$[R\cdot]_0$ a)	k_t b)	$[R\cdot]_0$	k_t
1	7.6	0.31	1.7×10^{-1}	3.1	1.7×10^{-2}
2	14.3	0.31	1.7×10^{-1}	3.1	1.7×10^{-2}
3	20.1	0.71	1.5×10^{-1}	7.1	1.5×10^{-2}
4	21.0	1.00	1.6×10^{-1}	10.0	1.6×10^{-2}
5	25.8	0.35	1.7×10^{-1}	3.5	1.7×10^{-2}

a) The unit of $[R\cdot]_0$ is M, see eq. (12). The k_p was assumed to be the same with the solution phase, 3.6×10^3 $M^{-1}\cdot s^{-1}$[2,3]. b) The unit of k_t is $M^{-1}\cdot s^{-1}$, see eq. (13).

The results of $[R\cdot]_0$ (2 nm) are very close to those from Baker et al.[4], who assumed the initiators were distributed over a height of approximately 2 nm.

If assuming a 100% initiation of the initial number of initiators and taking $h = 2$ nm, one has $[R\cdot]_0 = 4.2$ M.

$$[R\cdot]_0 = \frac{S_1}{S_0 N_A}\cdot\frac{1}{S_1 h} = \frac{1}{20\times10^{-20}\times6.02\times10^{23}\times2\times10^{-9}} = 4.2$$

This $[R\cdot]_0$ value leads to a maximum $a = 1.9\times10^{12}$ $mm^2\cdot s\cdot mol^{-1}$.

$$a = \frac{1}{k_p[M][R\cdot]_0} = \frac{1}{3.6\times10^3\times0.35\times4.2} = 1.9$$

For most cases, we had the fitted $a = 2$, corresponding to ~100% initiation of the initiator. In Table 9, $a = 0.004$ which is too much for the possible initiator on a QCM chip. We attributed this to two reasons: (i) our assumption that $[R\cdot]_0$ would not increase was no longer valid, (ii) the fitting gave a large error for small a values.

1 Ulman A. Formation and structure of self-assembled monolayers. Chem Rev, 1996, 96(4): 1533－1554

2 Coullerez G, Carlmark A, Malmström E, Jonsson M. Understanding copper-based atom-transfer radical polymerization in aqueous media. J Phys Chem A, 2004, 108(35): 7129－7131

3 Minko S, Sidorenko A, Voronov S, Gafijchuk G. Radical polymerization initiated from a solid substrate. 1. Theoretical background. Macromolecules, 1999, 32(14): 4525－4531

4 Kim J B, Huang W X., Miller M D, Baker G L, Bruening M L. Kinetics of surface-initiated atom transfer radical polymerization. J Poly Sci Part A, 2003, 41(3): 386－394